Chinese Chemical Letters 33 (2022) 2205–2211

Contents lists available at ScienceDirect

Chinese Chemical Letters

journal homepage: www.elsevier.com/locate/cclet

A green MXene-based organohydrogel with tunable mechanics and freezing tolerance for wearable strain sensors

Shuo Liu[a], Xinyu Tian[a], Xiansheng Zhang[a,b,c,*], Chongzhi Xu[a], Lili Wang[a,**], Yanzhi Xia[a]

[a] State Key Laboratory of Bio-Fibers and Eco-Textiles, College of Textiles and Clothing, Collaborative Innovation Center for Marine Biomass Fibers, Materials and Textiles of Shandong Province, Institute of Marine Biobased Materials, Qingdao University, Qingdao 266071, China
[b] Key Laboratory of Clean Dyeing and Finishing Technology of Zhejiang Province, Shaoxing University, Shaoxing 312000, China
[c] Research Center for Intelligent and Wearable Technology, Intelligent Wearable Engineering Research Center of Qingdao, Qingdao University, Qingdao 266071, China

ARTICLE INFO

Article history:
Received 30 July 2021
Revised 16 September 2021
Accepted 18 September 2021
Available online 24 September 2021

Keywords:
Organohydrogel
Mechanical performance
Temperature tolerance
Strain sensor
MXene

ABSTRACT

Conductive hydrogels have attracted considerable attention owing to their potential for use as electronic skin and sensors. However, the loss of the inherent elasticity or conductivity in cold environments severely limits their working conditions. Generally, organic solvents or inorganic salts can be incorporated into hydrogels as cryoprotectants. However, their toxicity and/or corrosive nature as well as the significant water loss during the solvent exchange present serious difficulties. Herein, a liquid-like yet non-toxic polymer-polyethylene glycol (PEG) was attempted as one of the components of solvent for hydrogels. In the premixed PEG-water hybrid solvent, polyacrylamide (PAAm) was *in situ* polymerized, overcoming the inevitable water loss induced by the high osmotic pressure of the PEG solution and achieving tailored water capacity. Interestingly, the mechanical strength ("soft-to-rigid" transition) and anti-freezing properties of organohydrogels can be simultaneously tuned over a very wide range through adjusting PEG content. This was due to that with increasing PEG in solvent, the PAAm chains transformed from stretching to curling conformation, while PEG bonded with water molecules *via* hydrogen bonds, weakening the crystallization of water at subzero temperature. Additionally, a highly conductive $Ti_3C_2T_x$-MXene was further introduced into the organohydrogels, achieving a uniform distribution triggered by the attractive interaction between the rich functional groups of the nanofillers and the polymer chains. The nanocomposite hydrogels demonstrate high electrical conductivity and strain sensitivity, along with a wide working temperature window. Such a material can be used for monitoring human joint movement even at low temperature and has potential applications in wearable strain sensors.

Hydrogels are characterized by a three-dimensional network, which is composed of chemically or physically crosslinked polymer chains, surrounded by a large amount of water [1–4]. Owing to their unique advantageous properties, including flexibility and high water content [5–8], they are widely used in various fields, such as tissue engineering and wearable electronics [9–13]. However, extreme environments severely limit the applications of hydrogels due to a reduction in their performance. In particular, under low-temperature conditions, traditional hydrogels freeze, and thus, their flexibility, conductivity, and transparency are lost [14–17]. To overcome this difficulty, in recent years, the development of anti-freezing hydrogels has attracted widespread attention.

As seen in the literature, the incorporation of cryoprotectants into hydrogels has become a popular approach for fabricating anti-freezing hydrogels. Cryoprotectants are mainly divided into the following three categories: (1) The freezing point of the water phase in the hydrogel can be effectively reduced by introducing inorganic salts (such as LiCl, $CaCl_2$ and $ZnCl_2$); these salts endow the hydrogel with anti-freezing properties [18,19]. Zhang *et al.* [20] introduced a mixture of $ZnCl_2/CaCl_2$ into the cellulose hydrogel network, and the obtained inorganic salt–water gel retained excellent stretchability and toughness at low temperature. Morelle *et al.* [18] added $CaCl_2$ to the popular polyacrylamide (PAAm)/alginate double-network hydrogel. The inorganic salts not only inhibited the formation of ice crystals at low temperature but also en-

* Corresponding author at: State Key Laboratory of Bio-Fibers and Eco-Textiles, College of Textiles and Clothing, Collaborative Innovation Center for Marine Biomass Fibers, Materials and Textiles of Shandong Province, Institute of Marine Biobased Materials, Qingdao University, Qingdao 266071, China.
** Corresponding author.
E-mail addresses: xshzhang@qdu.edu.cn (X. Zhang), llwang@qdu.edu.cn (L. Wang).

https://doi.org/10.1016/j.cclet.2021.09.063
1001-8417/

dowed the hydrogel with ionic conductivity. The hydrogel exhibited superior electrical and tensile properties at a temperature of −57 °C. (2) Inspired by the fact that plants in nature can survive in ultra-low temperature environments, researchers have developed a series of binary solvent systems (including ethylene glycol or glycerol/water, betaine or proline/water, and ammonium hydroxide/water) based on the mechanism that inhibits the freezing of water through the introduction of lipids into cell membranes. Organic solvents are usually introduced into the hydrogel using the solvent replacement method [21–24], producing what are known as "organohydrogels". Commonly used organic solvents include ethylene glycol (EG), dimethyl sulfoxide (DMSO), and glycerol [25,26]. Sui *et al.* [27] introduced zwitterionic penetrants (betaine and proline) into the hydrogel *via* solvent replacement. The resulting hydrogels exhibited excellent ionic conductivity at a temperature of −40 °C. The cationic groups of betaine and the anionic groups of proline formed hydrogen bonds with water molecules *via* electrostatic-induced hydration. This hydrogen bond formation destroyed the inherent hydrogen bond network between the water molecules and thus hampered the crystallization of the water molecules. Mo *et al.* [28] designed an anti-freezing hydrogel electrolyte by adding ethylene glycol monounsaturated fatty acid (EG-waPUA). Water molecules enhanced the interaction between the EG-WaPUA and the PAAm polymer chains. These interactions firmly locked the water molecules into the polymer network and disrupted lattice formation at low temperatures. Thus, the hydrogels obtained freezing resistance and maintained a high ionic conductivity at −20 °C. Ye *et al.* [29] used DMSO to induce the sol–gel conversion of a polyvinyl alcohol/cellulose nanofiber aqueous solution, in which hydrogen bonding interaction was formed between DMSO and the water molecules. The resulting hydrogels retained flexibility, conductivity, high stretchability, and high transparency at −70 °C. Liao *et al.* [30] immersed MXene nanocomposite hydrogels into EG to replace a part of the water molecules. Hydrogen bonds were generated between EG and the water molecules, which destroyed the formation of ice crystals and endowed the hydrogels with freezing resistance. A hydrogel with excellent self-healing ability, mechanical properties, and electrical conductivity at −40 °C was successfully fabricated using this method. (3) Anti-freezing hydrogels can be obtained through the combined use of inorganic salts and organic solvents. Lou *et al.* [31] designed a novel complex solvent system (EG/LiCl), where LiCl had high solubility in ethylene glycol. Under the joint action of inorganic salts and organic solvents, the obtained hydrogel maintained high toughness at −80 °C and electrical conductivity at −20 °C. The above investigations indicate that the introduction of organic solvents or inorganic salts using the solvent displacement method can endow hydrogels with improved anti-freezing properties, thus effectively broadening their working temperature range [32,33]. However, these methods and their practical applications still have some issues. For example, most of the cryoprotectant agents, especially in the case of organic anti-freezing solvents (such as EG and DMSO), are toxic, and some effective inorganic salts (such as LiCl) are corrosive. More importantly, the water content of the hydrogel is significantly reduced during the solvent replacement process, thus sacrificing their inherent high water content and flexibility. The challenge therefore remains to develop a nontoxic, anti-freezing hydrogel with controllable water content.

We note that single molecules of EG exhibit toxicity, but the toxicity is greatly reduced after polymerizing them into polymer polyethylene glycol (PEG). For this reason, a green non-toxic PEG was investigated as a possible anti-freezing agent. In this context, the significant loss of water content due to the osmotic pressure of PEG upon solvent replacement is a major challenge (Fig. S1 in Supporting information). Here, the PAAm monomer and auxiliary agents with better solubility in PEG were chosen, and the *in*

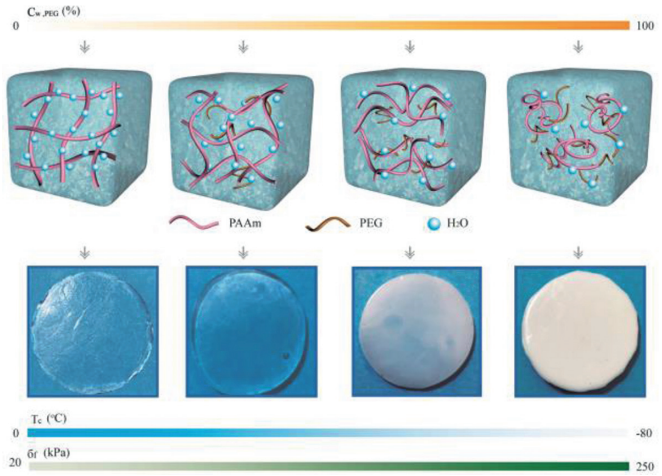

Fig. 1. Schematic diagram of the arrangement of polymer chains for PAAm PEG-based hydrogels. (a) $C_{w,PEG}$ = 0%. (b) $C_{w,PEG}$ = 50%. (c) $C_{w,PEG}$ = 60%. (d) $C_{w,PEG}$ = 80%. ($C_{w,PEG200}$ represents the concentration of PEG200, T_c represents the crystallization temperature of water in the hydrogel, and σ_f represents the breaking strength of hydrogel.)

situ polymerization was undertaken in the as-prepared PEG/H_2O binary solvent, thus successfully obtaining green organohydrogels with tailored water content. The influence of the molecular weight of PEG, the concentration of PEG in binary solvents, and the weight fraction of PAAm on the anti-freezing performance and mechanical properties was systematically explored. PAAm hydrogels were found to exhibit three states upon varying the PEG content in the binary solvents (Fig. 1). Within the low-PEG-content regime (Fig. 1b), a large number of water molecules were located around PAAm chains, giving the polymer chains a free state. In this case, the hydrogel was transparent and flexible, and its appearance was similar to that of the pure water PAAm hydrogel (Fig. 1a). With the increase in the PEG concentration (Fig. 1c), the number of water molecules around PAAm molecular chains was reduced, which was induced by the reduction of the water content and the attraction of water molecules to PEG, leading to the gradual approach of PAAm chains. Here, the mobility of the polymer chains and the transparency of the hydrogels decreased. When the PEG concentration reached its peak (Fig. 1d), rare water molecules could surround with PAAm chains. The phase separation of the PAAm chains was induced in this regime, leading to considerable curling of the polymer chains and thus the white appearance of the hydrogel. It is notable that, with the increase in the PEG concentration, the strength and anti-freezing performance of the hydrogels increased, but the resilience of the hydrogel gradually decreased. In summary, PEG molecules were introduced *in situ* to effectively regulate the aggregation of the polymer chains in hydrogels and were found to simultaneously generate a hydrogen bonding interaction with water molecules, achieving the tunability of mechanical properties and anti-freezing properties of the hydrogels.

The effects of the PEG concentration in the PEG/H_2O binary solvent and the molecular weight of PEG on the freezing resistance of the mixed solution are presented in Fig. 2. The phase diagram depicting the PEG concentration, temperature, and state of the PEG200/H_2O binary solvent is presented in Fig. 2a. The phase diagram is divided into three regions, namely, the liquid region (unfrozen state), the liquid–solid coexistence region (semi-frozen state), and the solid region (completely frozen state). The specific frozen state of the EG/H_2O and PEG/H_2O binary solvents with various values of $C_{w,EG}$ and $C_{w,PEG}$ was derived from their frozen state using a refrigerator at different temperatures (Fig. 2c and Fig. S2 in Supporting information). For example, with $C_{w,PEG200}$ = 60%,

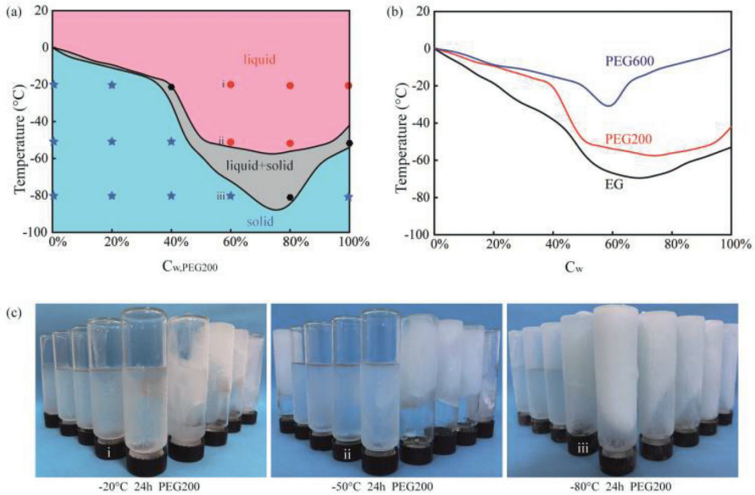

Fig. 2. (a) Phase diagram of constituents-temperature-frozen state for PEG200/H_2O binary solvent. (b) The effect of PEG molecular weight on the transition temperature of liquid state to liquid solid coexistence state. (c) The morphology of PEG200/H_2O binary solvent at different temperatures ($C_{w,PEG200}$ of binary solvent from left to right in each figure is 100%, 80%, 70%, 60%, 50%, 40%, 30%, 20% and 0%).

the mixed solution was found to remain in its liquid state when kept at a temperature of −20 °C for 24 h (Figs. 2c-i and a-i). The mixed solution also remained its liquid state (Figs. 2c-ii and a-ii) when exposed to −50 °C for 24 h, whereas it became solid when kept at −80 °C for 24 h (Figs. 2c-iii and a-iii). As the temperature decreased, the binary solvent first transitioned from a liquid state to a liquid–solid coexistence state and then transformed from the liquid–solid coexistence state to a solid state. The PEG concentration of the binary solvent played a significant role in determining its anti-freezing performance. Within the regime of $C_{w,PEG200} < 75\%$, the temperatures of the transitions from the liquid state to the liquid–solid coexistence state and from the liquid–solid coexistence state to the solid state of the binary solvent gradually decreased with the increase in $C_{w,PEG200}$, indicating an improved freezing resistance with increasing $C_{w,PEG200}$. When $C_{w,PEG200}$ was higher than 80%, the abovementioned transition temperatures gradually increased with the increase in $C_{w,PEG200}$, indicating that, above this threshold, the freezing resistance was gradually weakened with increasing $C_{w,PEG200}$. When $C_{w,PEG200}$ was in the range of 75%–80%, the mixed solution was still not completely frozen even when exposed to temperatures of −80 °C for 24 h (Fig. 2c), indicating that this solvent had the strongest freezing resistance. The correlation between the PEG concentration in binary solvents and the corresponding anti-freezing ability is due to the fact that, within the low-PEG-concentration regime, with the increase in the PEG concentration, more water molecules are capable of bonding with the PEG molecules forming hydrogen bonds. As a result, the number of free water molecules decreases, reducing the content of low-temperature-induced crystallized water molecules and thus enhancing the anti-freezing performance of the binary solvent. However, within the high-PEG-concentration regime (> 80%), the number of water molecules in the system decreases, and the number of free PEG molecules thus increases. In this case, more PEG molecules crystallize at low temperature, leading to the poor anti-freezing performance.

In addition, by comparing the transitions of the liquid state to the liquid–solid coexistence state for PEG/H_2O solvents with different PEG molecular weights (MW_{PEG}) (Fig. 2b), it can be observed that the temperature of the binary solvent state transition gradually increases with the increase in the PEG molecular weight. Under the same PEG concentration, the anti-freezing performance of the binary solvent becomes stronger with the decrease in MW_{PEG}. In most work reported in the literature, researchers adopt EG as an anti-freezing agent [26,30]. This may be due to the fact that, as the MW_{PEG} increases, PEG transforms from a colorless, viscous liquid state into a solid wax state. This transition is accompanied by a gradual increase in solution viscosity, which results in a significantly decreased solubility of PEG in binary solvents. In other words, for large MW_{PEG}, the dispersion degree of PEG and water molecules is reduced, and the water molecules cannot effectively bond with the PEG chains, leading to the observed poor freezing resistance of the mixed solution. Considering both the freezing resistance and solvent toxicity, PEG200 was selected as one component of the binary solvents used to prepare green anti-freezing organohydrogels.

In order to prepare the anti-freezing flexible PAAm hydrogel that can meet the requirements of low temperature environment in winter, northern cities (Heilongjiang, China, *etc.*) and Antarctica, PEG200/H_2O ($C_{w,PEG200}$ = 80%, 70%, 60%, 50%) with superior anti-freezing properties was chosen as the solvent. The mechanical performance of the PAAm PEG-based hydrogels is presented in Fig. 3. The stress–strain curves of the PAAm PEG-based hydrogels in the case of $C_{w,AAm}$ = 30% with different $C_{w,PEG}$ are presented in Fig. 3a. With increasing $C_{w,PEG}$, the fracture strength (σ_f) of the hydrogels increases, but the strain at breakage (ε_f) decreases, indicating a "soft-to-rigid" transition of the hydrogel. We therefore find that the mechanical parameters of the PAAm PEG-based hydrogels can be tuned over an extraordinarily broad range by varying the content of PEG in the binary solvent. For instance, when $C_{w,PEG}$ = 50%, the ε_f of the hydrogel was 10.5, whereas σ_f was only 50 kPa, indicating that the sample had the properties of a soft and flexible hydrogel. When $C_{w,PEG}$ increased to 80%, σ_f could reach 275 kPa, but ε_f was only 1, representing a rigid hydrogel. The influence of the PEG content in the binary solvent on the elastic recovery of the PAAm PEG-based hydrogels is presented in Fig. 3d. It can be observed that the area of the hysteretic circle in the tensile cycle curve significantly increases with the increase in strain, especially in the large $C_{w,PEG}$ regime, indicating the greater energy loss during loading and thus a lower elastic recovery rate of the hydrogel. Therefore, within the regime of low PEG content in the binary solvent, the hydrogel exhibits excellent elastic recovery. This is due to the fact that, with the increase in the PEG concentration in the binary solvent, the number of water molecules around the PAAm molecular chains decreases, which significantly reduces the mobility of the polymer chains. For this reason, the hydrogels exhibit reduced elastic recovery, higher strength, and a white

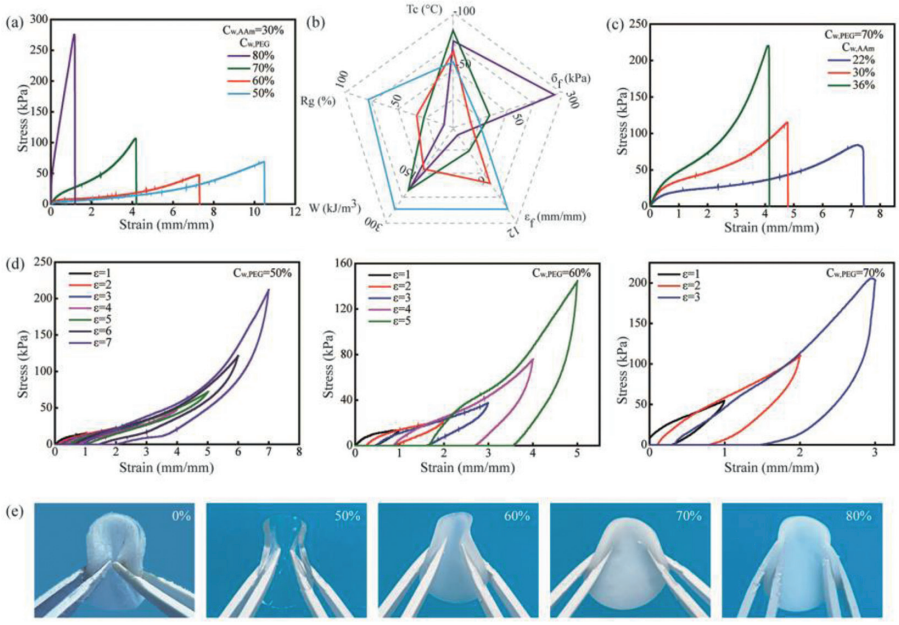

Fig. 3. (a) The stress-strain curves of PAAm PEG-based hydrogels ($C_{w,AAm}$ = 30%) prepared by different $C_{w,PEG}$. (b) Comparison of fracture strength, fracture strain, fracture energy, elastic recovery rate and freezing point of hydrogels in Fig. 3a. (c) The stress-strain curves of PAAm PEG-based hydrogels ($C_{w,PEG}$ = 70%) prepared by different $C_{w,AAm}$. (d) The tensile cycle curves of PAAm PEG-based hydrogels ($C_{w,AAm}$ = 30%) with $C_{w,PEG}$ = 50%, 60% and 70%, respectively. (e)The bending morphology of PAAm PEG-based hydrogels ($C_{w,AAm}$ = 30%) with different $C_{w,PEG}$ after frozen at −50 °C for 24 h.

appearance (Fig. 3e). The bending performance of the PAAm PEG-based hydrogels frozen at −50 °C for 24 h varied according to their different $C_{w,PEG}$ (Fig. 3e): the hydrogel with $C_{w,PEG}$ = 0% became white; this color arose from the low-temperature-induced crystallization of water molecules. In this case, the hydrogels lost flexibility, and some cracks caused by bending appeared in the samples. This indicates that the neat PAAm hydrogels cannot be used in low-temperature environments; such a restriction is a common issue in hydrogels. However, using PEG/H_2O as the solvent, the obtained hydrogels can be bent freely even at a low temperature.

To explore the effect of the AAm content ($C_{w,AAm}$) on the ultimate performance of the PAAm hydrogels, the binary solvent ($C_{w,PEG}$ = 70%) with the best anti-freezing performance was chosen, and the mechanical properties obtained with varying $C_{w,AAm}$ were established (Fig. 3c). As can be seen from the Fig. 3c, with the increase in $C_{w,AAm}$, the fracture strength of the hydrogels gradually increases, but the fracture strain decreases. In the case of low $C_{w,AAm}$, a low density of polymer chains or a sufficient number of water molecules around the polymer chains leads to weak polymer entanglement and hydrogen bonding interactions, giving rise to a high mobility of the PAAm chains and thus the ductile nature of the hydrogel. When $C_{w,AAm}$ becomes too high, the increased density of polymer chains or the reduced number of water molecules around the PAAm chains enhances polymer entanglement and hydrogen bonding interactions, resulting in a decreased mobility of the polymer chains and thus a poor elasticity of the hydrogels. It was thus found that the mechanical parameters of the PAAm PEG-based hydrogels can be regulated in a wide range by adjusting $C_{w,AAm}$.

In conclusion, we compare the properties of hydrogels with different PEG concentrations (Fig. 3b): the hydrogels with $C_{w,PEG}$ = 50% exhibit fracture strain of 10.5, fracture strength of 50 kPa, toughness of 258 kJ/m^3, and elastic recovery rate of 80%. The obtained hydrogels demonstrate high flexibility, ductility, and resilience and have a freezing point of as low as −60 °C. These flexible hydrogels are ideal candidates for wearable strain sensors, and their inherent flexibility, elastic recovery, and environmental stability are prerequisites for this application. To demonstrate this possible application, the aforementioned hydrogels with $C_{w,PEG}$ = 50% and $C_{w,AAm}$ = 30% were chosen for use as a matrix for flexible sensors. Furthermore, MXene, a two-dimensional material with excellent electrical conductivity, was introduced into the PAAm PEG-based hydrogels to fabricate an organohydrogel sensor, which can be used in cold environments.

To demonstrate the possible use of the obtained anti-freezing organohydrogels in the field of wearable sensor, the two-dimensional materials, MXene nanosheet, were fabricated using the HF etching method; they were characterized by a large specific surface area and short ion transport path [34,35]. In addition, the rich functional groups (−OH, −O, −F) [36,37] on the surface of MXene endowed it with high hydrophilicity, which facilitated their dispersion and strong combination with the organohydrogels. The MXene nanosheets were incorporated into the PAAm PEG-based hydrogels *via in situ* polymerization, making a conductive organohydrogel sensor with high resistance to freezing. After the removal of aluminum atoms in the MAX phase (Ti_3AlC_2) using an etching agent, the −OH, −O and −F groups in the solution were combined with the bonded unsaturated MX layer units to form MXene. In the transmission electron microscopy (TEM) and atomic force microscopy (AFM) images (Figs. 4a and b, respectively), ultra-thin nanosheets with good elimination can be observed. These nanosheets exhibit a single-layer structure with a thickness of about 1.5 nm. These features offer effective MXene conductive pathways in the organohydrogels and thus provide good conductivity to the organohydrogels.

After the MXene nanosheets were embedded in the PAAm PEG-based hydrogels, the obtained nanocomposite hydrogels demonstrated excellent flexibility (Fig. 4c). The overall uniform black appearance of the organohydrogels indicates that MXene nanosheets were evenly distributed in the organohydrogels. This was induced by the formation of a large number of hydrogen bonds between the hydroxyl groups on the surface of MXene and the amino groups in the PAAm chains or the hydroxyl groups in the polyethylene glycol chains (Fig. 4d). This bond formation promotes a high

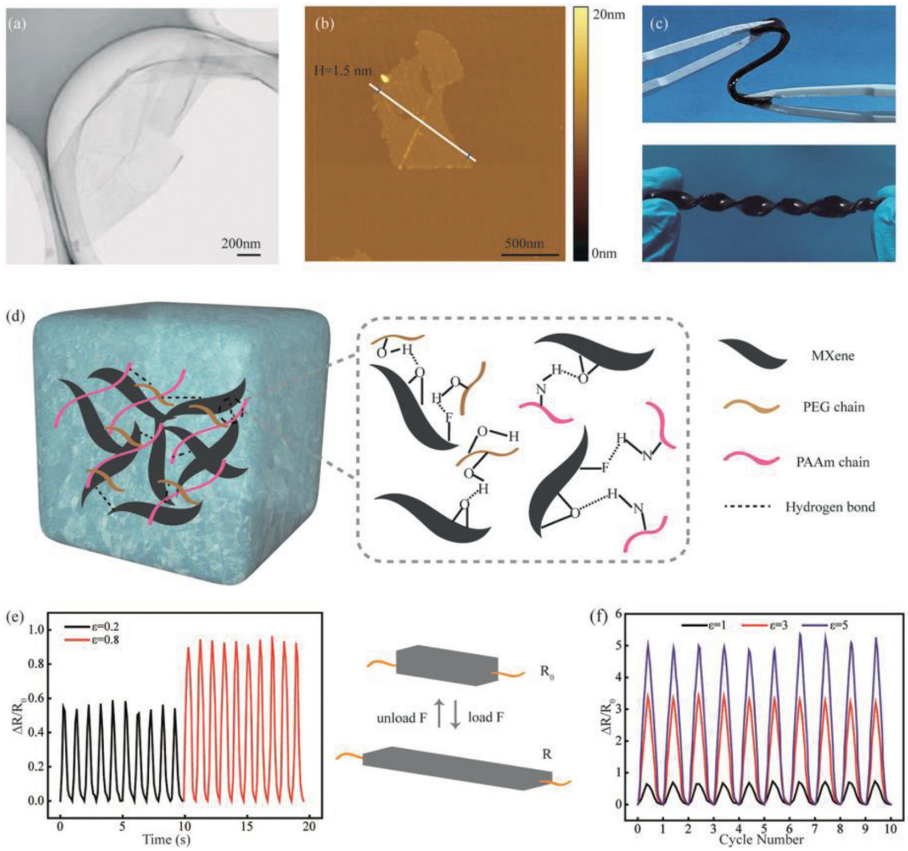

Fig. 4. The TEM (a) and AFM (b) images of MXene nanosheets. (c) The display of flexible PAAm/MXene PEG-based organohydrogels at room temperature. (d) The mechanism of better dispersion of MXene in the organohydrogels. The changes of relative resistance for PAAm/MXene PEG-based organohydrogels at small strain (e) and large strain (f) tensile cycles.

dispersion of MXene in the organohydrogel matrix and strong bonding with the organohydrogel matrix (Fig. 4c). This strong interaction could be further confirmed by the mechanical properties of PAAm/MXene PEG-based hydrogels (Fig. S3 in Supporting information). When MXene was introduced, the fracture strength of hydrogels increased and the fracture strain decreased to a certain extent. Therefore, the addition of MXene could improve the mechanical strength of the PAAm/MXene PEG-based hydrogels. Tensile cycle testing was also conducted on the nanocomposite organohydrogels in the regime of small (0.2 and 0.8) and large strains (1, 3 and 5) while simultaneously evaluating their electromechanical properties. As can be seen from Fig. 4e, the organohydrogel has high strain sensitivity in the low-strain regime (tested with strains of 0.2 and 0.8), and $\Delta R/R_0$ demonstrates good stability and reproducibility over prolonged testing. To further test the electromechanical properties under large strain, strains of 1, 3 and 5 were selected for tensile cycle testing to obtain the $\Delta R/R_0$ variations (Fig. 4f). It can be seen that, in the initial phase of testing, the resistance almost completely recovers, and with the increase in strain, $\Delta R/R_0$ gradually increases, indicating the sensitivity and long-term electrical stability of the sensor. These properties arise from the fact that the nanocomposite organohydrogels with $C_{w,PEG} = 50\%$ and $C_{w,AAm} = 30\%$ have excellent ductility and elastic recovery (Fig. 3), which enable the organohydrogels to maintain the integrity of structure even when exposed to large strain. This ensures that the electrical signal can be effectively and repeatedly transmitted. It should be pointed out that $\Delta R/R_0$ slightly increases with the increase in the number of cycles at a large strain of 5. This may be due to the deterioration of the microstructure of the nanocomposite organohydrogels caused when the external strain exceeds the critical value. This critical value is observed where the continuous MXene nanosheets are separated to some degree, and a simultaneous increase in the resistance for the conductive path is observed at this critical strain. In summary, the PAAm/MXene PEG-based organohydrogels demonstrate high strain sensitivity, which thus makes them excellent candidates for use as strain sensors.

To evaluate the working ability of the above hydrogels under extreme conditions, the stability of the PAAm/MXene PEG-based organohydrogels at low temperature was also investigated. When the hydrogels were frozen at −20 °C for a long time of 24 h, the nanocomposite hydrogels could still bend freely and achieve complex shapes (Fig. 5a). This indicates that the PAAm/MXene PEG-based organohydrogels retained their excellent flexibility even at low temperature, thus meeting the deformation requirements of wearable sensors. Additionally, in order to simulate the sensing performance at low temperature as much as possible, the PAAm/MXene PEG-based organohydrogels were frozen in the refrigerator (−20 °C) for a sufficient time of 24 h. After that, the hydrogels were taken out immediately and the measurements of sensing performance was collected, where the whole process took about 1, 2 min and guaranteed the low temperature of hydrogels. According to the electromechanical properties under tensile cyclic loading (Fig. 5b), the nanocomposite hydrogels retain their strain sensitivity and electrical stability at a low temperature. The relative resistance before and after freezing does not significantly change. The PAAm/MXene PEG-based organohydrogels prepared in this work demonstrated to have high flexibility (Fig. 5a) and conductivity (Fig. 5b), thus making them an ideal candidate for strain sensors [38–40]. These PAAm/MXene PEG-based organohydrogels have many exceptional properties, including good

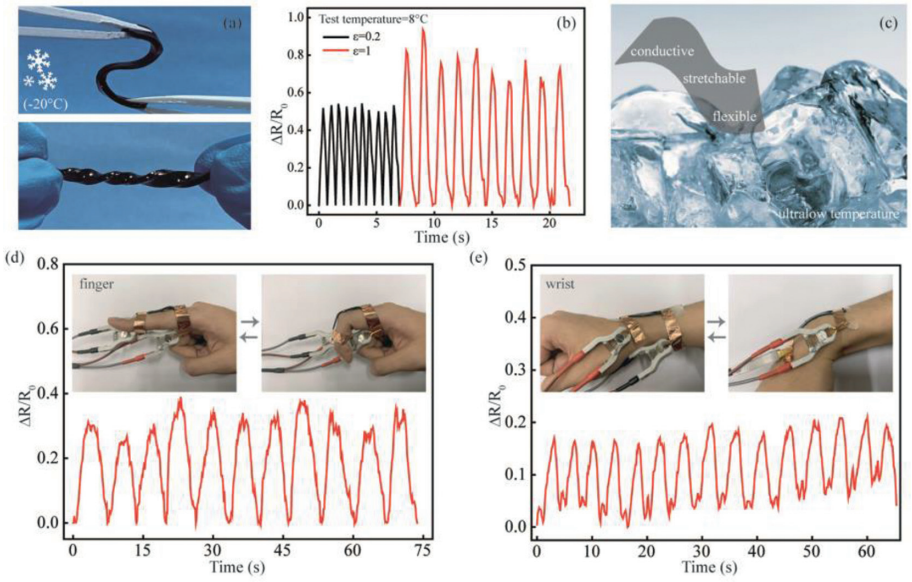

Fig. 5. (a) The display of flexible PAAm/MXene PEG-based organohydrogels after frozen at −20 °C for 24 h. (b) The electromechanical properties of PAAm/MXene PEG-based organohydrogels after freezing at −20 °C for 24 h. (c) The schematic diagram of anti-freezing PAAm/MXene PEG-based organohydrogels strain sensor. The applications of PAAm/MXene PEG-based organohydrogels for detection of human motions. The changes of relative resistance with bend of (d) finger and (e) wrist.

extendibility, toughness, elastic recovery, sensitivity, electrical stability, and freezing resistance (Fig. 5c). In view of these properties, the proposed PAAm/MXene PEG-based organohydrogels have high application potential in the field of wearable sensing devices. With this application in mind, a hydrogel strain sensor was attached to the joints of the human body using an adhesive tape and used to monitor joint motion by observing the value of $\Delta R/R_0$. As presented in Fig. 5d, an organohydrogel strain sensor was attached to a joint on the finger. When the finger was bent by 90°, a simultaneous increase in the relative resistance was observed. In addition, the resistance variations exhibited high repeatability, indicating that the strain sensor has high stability and a rapid response ability. Subsequently, the motion of the wrist joint was monitored using the same method (Fig. 5e), and similar variations in resistance were observed. This work indicates that the PAAm/MXene PEG-based organohydrogel strain sensors can be used to detect human motion. They also have potential applications in the fields of flexible, wearable electronic devices and sensors.

In conclusion, a green anti-freezing PAAm organohydrogel and the corresponding strain sensor were prepared *via in situ* polymerization using a non-toxic liquid-like polyethylene glycol as one component of the solvent. The addition of PEG not only regulates the conformation and aggregation state of the PAAm chains but also forms hydrogen bonds with the water molecules, which effectively suppressed the crystallization of water. Therefore, the simultaneous tuning of the mechanical properties and freezing resistance of the hydrogels are achieved by altering PEG content. Considering the tensile properties and resilience of the anti-freezing hydrogels, and with the aim of increasing the functionality of the hydrogels, a highly conductive MXene was introduced into the PAAm PEG-based "organohydrogels". Interestingly, the MXene nanosheets uniformly distributed in the hydrogel matrix induced by the formation of hydrogen bonds between the functional groups on the surface of MXene and the PAAm chains. The resulting PAAm/MXene nanocomposite organohydrogels demonstrated excellent conductivity and strain sensitivity, which has potential application in the monitoring of human joint motion. This research provides a new method for the preparation of green, anti-freezing, and flexible hydrogel sensors, which have potential application in wearable electronic devices, electrodes, and sensors.

Declaration of competing interest

The authors declare that they have no known competing financial interests or personal relationships that could have appeared to influence the work reported in this paper.

Acknowledgments

The current work was financially supported by the National Natural Science Foundation of China (Nos. 51803101 and 52003131), Natural Science Foundation of Shandong Province (Nos. ZR2019BEM005 and ZR2019BEM026), China Postdoctoral Science Foundation (No. 2021T140352), State Key Laboratory of Bio-Fibers and Eco-Textiles (Qingdao University, Nos. ZKT14, ZKT32, GZRC202016, ZFZ201805), Project of Key Laboratory of Clean Dyeing and Finishing Technology of Zhejiang Province (No. QJRZ1904), Program for Changjiang Scholars and Innovative Research Team in University (No. IRT_14R30) and Taishan Scholar Program of Shandong Province (No. tspd20181208).

Supplementary materials

Supplementary material associated with this article can be found, in the online version, at doi:10.1016/j.cclet.2021.09.063.

References

[1] H. Yuk, B. Lu, X. Zhao, Chem. Soc. Rev. 48 (2019) 1642–1667.
[2] Z. Xiong, C. Zheng, F. Jin, et al., Sens. Actuator. B: Chem. 274 (2018) 541–550.
[3] R. Suris-Valls, I.K. Voets, Int. J. Mol. Sci. 20 (2019) 5149.
[4] C. Zheng, F. Jin, Y. Zhao, et al., Sens. Actuators B: Chem. 304 (2020) 127345.
[5] L.L. Wang, X.S. Zhang, Y.Z. Xia, et al., Adv. Mater. 31 (2019) 1902381.
[6] X.W. Zhao, M. Ding, C.Z. Xu, et al., Carbohydr. Polym. 251 (2021) 117054.
[7] L.L. Wang, X.W. Zhao, X.S. Zhang, et al., Chem. Eng. J. (2021) 405.
[8] X.B. Hou, Z.X. Xue, Y.Z. Xia, et al., Int. J. Biol. Macromol. 125 (2019) 1289–1298.
[9] P. Wei, T. Chen, G. Chen, et al., ACS Appl. Mater. Interfaces 12 (2020) 3068–3079.
[10] S. Zhang, S. Li, Z. Xia, K. Cai, J. Mater. Chem. B 8 (2020) 852–862.
[11] H.R. Lim, H.S. Kim, R. Qazi, et al., Adv. Mater. 32 (2020) 1901924.
[12] J.S. Chen, Q.Y. Peng, T. Thundat, H.B. Zeng, Chem. Mater. 31 (2019) 4553–4563.
[13] J.W. Li, D.D. Yuan, X.J. Zheng, et al., Sci. China Chem. 63 (2020) 546–553.
[14] D. Chen, X. Zhao, X. Wei, et al., ACS Appl. Mater. Interfaces 12 (2020) 53247–53256.
[15] M. Hua, S. Wu, Y. Ma, et al., Nature 590 (2021) 594–599.

[16] W. Wang, Y. Liu, S. Wang, et al., ACS Appl. Mater. Interfaces 12 (2020) 25353–25362.
[17] S. Wu, M. Hua, Y. Alsaid, et al., Adv. Mater. 33 (2021) 2007829.
[18] X.P. Morelle, W.R. Illeperuma, K. Tian, et al., Adv. Mater. 30 (2018) 1801541.
[19] Y. Bai, B. Chen, F. Xiang, et al., Appl. Phys. Lett. 105 (2014) 151903.
[20] X.F. Zhang, X. Ma, T. Hou, et al., Angew. Chem. Int. Ed. 58 (2019) 7366–7370.
[21] C.Z. Xu, S. Liu, X.W. Zhao, et al., ACS Appl. Mater. Interfaces 13 (2021) 25383–25391.
[22] L. Han, K.Z. Liu, M.H. Wang, et al., Adv. Funct. Mater. 28 (2018) 1704195.
[23] F. Chen, D. Zhou, J. Wang, et al., Angew. Chem. Int. Ed. 57 (2018) 6568–6571.
[24] J. Song, S. Chen, L. Sun, et al., Adv. Mater. 32 (2020) 1906994.
[25] C. Lu, X. Chen, Nano Lett. 20 (2020) 1907–1914.
[26] Q. Rong, W. Lei, L. Chen, et al., Angew. Chem. Int. Ed. 56 (2017) 14159–14163.
[27] X.J. Sui, H.S. Guo, P.G. Chen, et al., Adv. Funct. Mater. 30 (2019) 1907986.
[28] F.N. Mo, G.J. Liang, Q.Q. Meng, et al., Energy Environ. Sci. 12 (2019) 706–715.
[29] Y.H. Ye, Y.F. Zhang, Y. Chen, X. Han, F. Jiang, Adv. Funct. Mater. 30 (2020) 2003430.
[30] H. Liao, X.L. Guo, P.B. Wan, G.H. Yu, Adv. Funct. Mater. 29 (2019) 1904507.
[31] D. Lou, C. Wang, Z. He, et al., Chem. Commun. 55 (2019) 8422–8425.
[32] M.S. Zhu, X.J. Wang, H.M. Tang, et al., Adv. Funct. Mater. 30 (2019) 1907218.
[33] X. Fan, W. Zhou, Y. Chen, et al., ACS Appl. Mater. Interfaces 12 (2020) 32031–32040.
[34] X.T. Jiang, A.V. Kuklin, A. Baev, et al., Phys. Rep. Rev. Sec. Phys. Lett. 848 (2020) 58.
[35] C.B. Liang, H. Qiu, P. Song, et al., Sci. Bull. 65 (2020) 616–622.
[36] L. Ding, L.B. Li, Y.C. Liu, et al., Nat. Sustain. 3 (2020) 296.
[37] A. Sarycheva, Y. Gogotsi, Chem. Mater. 32 (2020) 3480–3488.
[38] J. Gu, J. Huang, G. Chen, et al., ACS Appl. Mater. Interfaces 12 (2020) 40815–40827.
[39] Z.W. Jiang, Y.S. Wang, G.Q. Xu, et al., Chin. Chem. Lett. 33 (2022) 1011–1016.
[40] J.H. Bai, R. Wang, M.X. Ju, et al., Sci. China Mater. 64 (2020) 942–952.